Fuel 252 (2019) 148–156

Contents lists available at ScienceDirect

Fuel

journal homepage: www.elsevier.com/locate/fuel

Full Length Article

Novel methods of sewage sludge utilization for photocatalytic degradation of tetracycline-containing wastewater

Xuefeng Zhu[a,b], Wenyi Yuan[c], Maoqian Lang[a], Guangyin Zhen[d,e,*], Xuedong Zhang[b,*], Xueqin Lu[d,f]

[a] School of Environmental and Material Engineering, Shanghai Polytechnic University, Shanghai 201209, PR China
[b] Section Sanitary Engineering, Department of Water Management, Faculty of Civil Engineering and GeoSciences, Delft University of Technology, 2628CN Delft, Netherlands
[c] Shanghai WEEE Recycling Collaborative Innovation Center, Shanghai 201209, PR China
[d] Shanghai Key Lab for Urban Ecological Processes and Eco-Restoration, School of Ecological and Environmental Sciences, East China Normal University, Shanghai 200241, PR China
[e] Shanghai Institute of Pollution Control and Ecological Security, 1515 North Zhongshan Rd. (No. 2), Shanghai 200092, PR China
[f] Institute of Eco-Chongming (IEC), 3663 N. Zhongshan Rd., Shanghai 200062, PR China

GRAPHICAL ABSTRACT

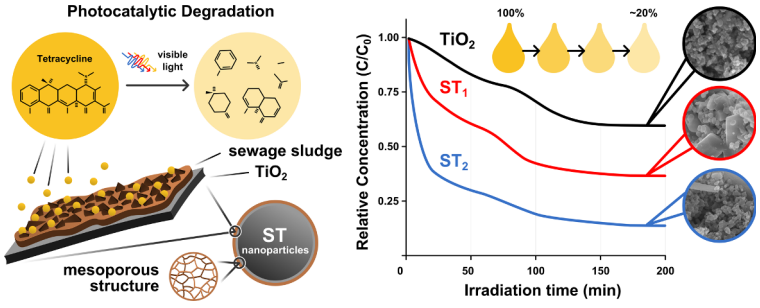

ARTICLE INFO

Keywords:
Photocatalytic activity
Tetracycline
TiO_2 photocatalysts
Sewage sludge
Reutilization

ABSTRACT

Two types of novel municipal sewage sludge (SS) combined TiO_2 photocatalysts (ST_1 and ST_2) were synthesized through calcination treatment under different atmospheres (air and N_2). The morphology, structure, and chemical states of photocatalysts were characterized by SEM, XRD, EDS, FT-IR, Raman UV–Vis, BET, and TG-IR. The results showed that ST_2 consisted of a mesoporous graphene-like structure (20.02 nm) displayed exhibited better visible light photocatalytic performances and the highest BET surface area and pore volume (92.97 $m^2 g^{-1}$ and 0.46 cm^3/g). The doping of Carbon and transition metals (Al, Mg) in TiO_2 strengthened visible-light response by lowering the band gap. The photocatalytic ability is evaluated in the degradation of tetracycline, which is a typical antibiotic in the aquatic environment. The ST_2 photocatalytic efficiency under visible light than that of ST_1 and TiO_2. The enhancement is formed together by porous surface and lower band gap of ST_2, which could offer more active sites and facilitate faster electron-hole pair separation. In addition, the sludge-TiO_2 calcination in N_2 (ST_2) has the potential to reduce CO_2 emission while recovering more energy from the sludge, which turned out to be a more cost-effective way to reutilization of sewage sludge compared with that of calcination in air.

* Corresponding authors at: Shanghai Key Lab for Urban Ecological Processes and Eco-Restoration, School of Ecological and Environmental Sciences, East China Normal University, Shanghai 200241, PR China (G. Zhen).
E-mail addresses: gyzhen@des.ecnu.edu.cn (G. Zhen), X.Zhang@tudelft.nl (X. Zhang).

https://doi.org/10.1016/j.fuel.2019.04.093
Received 9 January 2019; Received in revised form 6 April 2019; Accepted 16 April 2019
Available online 22 April 2019

1. Introduction

Sludge, which is an inevitable byproduct of numerous domestic and industrial activities, is considered deleterious to ecosystems [1]. Traditional methods of sludge disposal, such as landfills, open stack, incineration, and ocean discharge, are unable to effectively deal with the large volumes of sludge while meeting the increasingly stringent standards for sludge treatment and disposal [2,3]. Moreover, most municipal sludge contains organic matter, nitrogen, phosphorus, and other nutrients, as well as heavy metals, such as zinc, copper, nickel, lead, and chromium [4]. Therefore, it is important to exploit novel methods of sewage sludge (SS) utilization to ensure sustainable sludge treatment [5].

In recent years, applied research has raised concerns over the use of titanium dioxide (TiO_2) and other semiconductor catalysts for photocatalytic oxidation for removing organic pollutants and reducing heavy metal ions [6–9]. However, there are two main drawbacks hindering wide applications of the TiO_2 photocatalytic process in wastewater treatment, including the inefficient utilization of solar energy and the low adsorption of the contaminants in liquid [3,10]. Several previous studies calcined TiO_2 with sludge to synthesize novel TiO2 photocatalysts to efficiently overcome the aforementioned technical problems [1,2,11]. Such photocatalysts have three main advantages. Firstly, organic constituents of the sludge could result in the catalytic material developing a porous structure and a large Brunauer, Emmett, and Teller model calculation (BET) surface area, which increases the adsorption efficiency of the photocatalyst for contaminants [2,11–13]. Secondly, the inorganic constituents of sludge can be used as inorganic templates for TiO2 to increase the architecture stability of the TiO_2 photocatalysts and efficiency of light capture [11,14]. Lastly, transition metals in sludge such as dopant may accelerate the rate of separation of electrons and holes, which reduces the recombination rate of light-generated electrons and light-born holes and extends the catalytic efficiency [15]. Although the above-mentioned efforts have shown some success in the use of sludge-TiO_2 photocatalysts for the contaminant treatment in the aquatic environment, the information on the underlying changes of synthesis conditions in the characteristic of sludge-TiO_2 photocatalysts is limited. Some researchers had used the different atmosphere (mostly, N_2 and air) during the sludge-TiO_2 synthesis process [2,11,16]. This can be associated with the difference of combustion (oxidizing gas, air) and pyrolysis (inter-gas, N_2) of sludge [17]. Therefore, the different calcination gas occurs during the sludge-TiO_2 synthesis process, which can exert significant influences on the change of photocatalysts property and further industrial applications.

In China, over 8000 tons of antibiotics are currently used as feed additives each year [18]. Tetracycline (TC) is a typical antibiotic excreted into surface water and manure [19,20]. However, remediation techniques that are employed for the removal of antibiotic compounds from environmental media have several problems, such as low reduction efficiency with conventional biological processes and the high cost of equipment and the energy required for ozonation and Fenton's oxidation [18,21,22]. Therefore, it is imperative to identify an energy-efficient and environmentally friendly technology to effectively remove trace amounts of antibiotics in the aquatic environment.

The main objectives of this study were: 1) to prepare sludge-TiO_2 photocatalytic materials by the thermal-alkaline method under different protective gases (air and N_2); 2) to investigate the differences in their texture properties, crystalline phases, and chemical compositions using different techniques (including SEM, XRD, EDS, FT-IR, Raman UV–Vis, BET, and TG-IR); and 3) to evaluate the photocatalytic activities of the samples prepared above during treating tetracycline-containing wastewater under visible light irradiation.

2. Materials and methods

2.1. Reagents and materials

Waste activated sludge with a moisture content of 99.4% was obtained from the municipal wastewater treatment plant in Shanghai, China. The sludge was obtained from a secondary clarifier in which gravity thickening occurs following centrifugal dewatering. The Measurements of moisture content of sewage sludge were performed in accordance with the Chinese NEPA standard methods [23]. The sludge was first dewatered by a vacuum pump (moisture content of 90%) and dried at 105 °C for 48 h (until a moisture content of 2%). The dried SS material was ground by a grinding mill and sieved through a 40 mesh. The employed P25 TiO_2 (80% anatase, 20% rutile) was manufactured by Degussa (Germany).

The mineralogical data obtained from the dried SS samples were analyzed by X-ray fluorescence (XRF) using a spectrometer (Shimadzu XRF-1800, Japan). During the analysis of components of SS by XRF, elements such as Ca, Si, Fe, P, and S were detected with atomic ratios of 20.49%, 20.05%, 18.42%, 11.50%, and 8.29%, respectively. The present transition metals were displayed as the dopants for TiO_2 to improve the light-absorbing ability and electron-hole pair separation [11,24].

2.2. Photo-catalyst preparation

TiO_2 particles were integrated with SS for the preparation of the photo-catalyst and were processed using the thermal-alkaline method as described by previous research [2,25]. According to a mass ratio of SS: TiO_2: NaOH of 6:1:1, 6 g municipal sewage sludge and 1 g TiO_2 were first added into a 250 mL beaker containing 100 mL of distilled water. Subsequently, approximately 1 g of NaOH was dissolved in the mixture and stirred to result in a strong alkaline condition. After complete mixing, the compounds were transferred into a reaction kettle (Teflon vessel) and heated at 200 °C for 20 h. Distilled water and HCl were then added, and the pH of the mixture was adjusted to 7.0. The mixture was filtered through a 0.45 μm pore-size-filter membrane, following which the precipitate was washed with about 20 L distilled water and dried at 80 °C for 12 h. Then, the ST_0 samples were heated at 600 °C for about 0.5 h under different atmospheric conditions (air and N_2) to obtain the photocatalysts of ST_1 and ST_2, respectively. Finally, the photo-catalyst samples were dried and ground into fine powders to store under the indoor environment (about 22 °C) for two weeks before the analysis.

2.3. Photo-catalyst characterization

TG-FTIR experiments were conducted by TG 209 thermogravimetric analyzer system (Netzsch, Germany) coupled with a Vertex70 spectrometer Fourier transform infrared spectrometer (FTIR) (Bruker, Germany). About 20 mg of dried samples were heated in aluminum crucibles with the following atmosphere and temperature changing program: 1) during the first 20 min, temperature of 20 °C was increased to 600 °C at a rate of 30 K·min^{-1} and under N_2 atmosphere; 2) a constant temperature of 600 °C was maintained for 30 min under N_2 atmosphere; 3) a constant temperature of 600 °C was maintained for 10 min under a new atmospheric condition (air, mixture of N_2 (70%) and O_2 (30%)). This atmosphere and temperature profile was used since it is closest to the photocatalyst preparation process. The carrier gas flow rate was 30 mL·min^{-1}. The buoyancy effect of TG was removed by subtracting a blank test. The differential thermogravimetric (DTG) curves were obtained by numerical derivation of the TG curves. The gaseous products from the pyrolysis of sewage sludge in TGA were determined using FTIR spectra. The transfer line and gas cell were

heated to a temperature of 200 °C to avoid condensation of volatile decomposition products. The wave number range of IR was 4000–600 cm^{-1}. The resolution and sensitivity were set at 4 cm^{-1}, and the spectrum scan frequency was 8 times per minute.

The BET surface area of the samples were measured using a Micromeritics instrument (ASAP 2020). The photocatalytic micromorphology of TiO_2 particles combined with SS was observed under an S-4800 SEM (Hitachi, Japan), which was operated at 10 kV. Elemental composition was determined by INCA X-Act energy-dispersive spectroscopy (EDS). The crystalline structure was analyzed using the XRD with a D8 Advance X-ray diffractometer (Bruker, Germany) under Cu Ka radiation (k = 0.154 nm) operated at 40 kV and 40 mA. Ultraviolet–visible (UV–Vis) measurement (UV-2550, Shimadzu, Japan) was obtained by means of the spectrophotometer with an integrating sphere accessory for diffuse reflectance in the range of 200–800 nm, and $BaSO_4$ was applied as the standard for these measurements. The method using KBr tablet was employed in the Fourier transform infrared spectroscopy (FT-IR) analysis (Vertex70, Bruker, Germany). Regardless of organic residues on the surface, the sample was prepared by combining sludge with TiO_2 finely pressed into sheets by FT-IR. Using the VERTEX 70 Raman spectra (Bruker, Germany) in the range of 200–4 000 cm^{-1}, samples were curve-fitted to confirm the crystalline and amorphous structure. The Micro-Raman spectra were measured at room temperature with a 532 nm laser line as the excitation source.

2.4. Photo-irradiation of tetracycline

The photocatalytic activities of the samples were evaluated in terms of tetracycline degradation with a photocatalytic reactor (XPA-II, Xu Jiang, China). An 800 W Xe lamp, mainly emitting visible light in the range of 400–800 nm, was used as the light source and placed in a quartz socket tube. Water was circulated through the interlayer to cool the system and magnetic stirring was used to suspend the photocatalyst in the reaction solution. Approximately 100 mL of tetracycline aqueous solution (5 $mg{\cdot}L^{-1}$) and 10 mg of either ST_1 or ST_2 sample was placed in quartz glass tubes. The suspension was stirred in the dark for 1 h to ensure an adsorption–desorption equilibrium and then the photocatalyst was separated and exposed to irradiation in a solution. Every periodic interval, 2.0 mL of the suspensions was collected, centrifuged, and detected using a UV–vis spectrophotometer (UV-2550, Shimadzu, Japan). All the above analyses were conducted in duplicate, and their average values were reported.

The maximum absorption at a wavelength of 275 and 350 nm was used to calculate the degradation rate in Fig. S1a [26]. The correlation coefficient (R^2) between antibiotic concentration and absorbance was 0.99 (Fig. S1b). This suggests that the absorbance value is an indirect indicator of tetracycline concentration. The tetracycline removal was determined using Eq. (1):

$$\text{Removal}\,(\%) = (C_0 - C_t) \times 100 \quad (1)$$

where C_0 and C_t are the concentrations of TC before and after the photocatalytic reaction, respectively.

3. Results and discussion

3.1. Morphology of sludge-derived TiO_2 photocatalysts

SEM images in Fig. 1 showed the morphology of TiO_2 particles that were attached to the structure of the SS. A clump of the TiO_2 particles was found shown to be spread on the surface of the SS. The shape of the TiO_2 particles had changed to a sheet-like structure on the surface of the sludge after the thermal-chemical treatment. The SEM images of the completed TiO_2 and the municipal SS were obtained. These two setups differed in their gas atmosphere of calcination, which resulted in

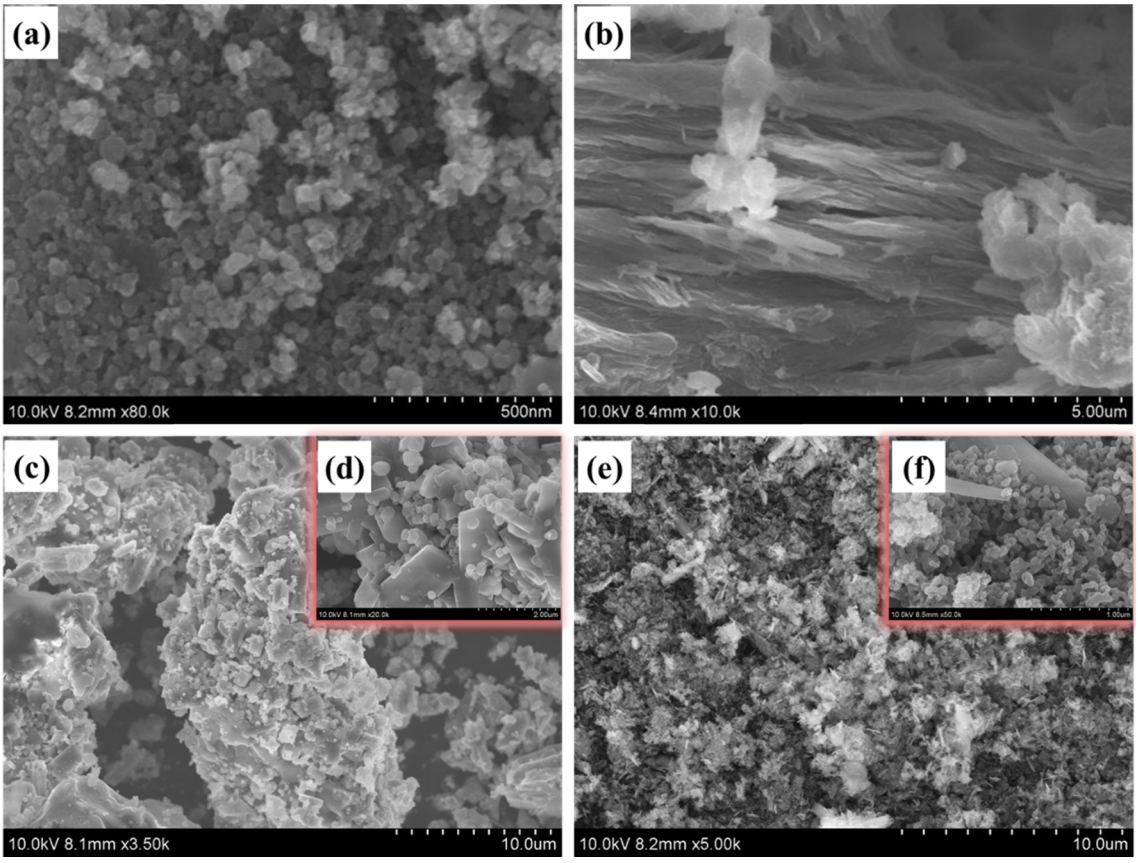

Fig. 1. SEM images of (a) TiO_2 mixed with SS, (b) TiO_2 with sludge and NaOH at 200 °C, ((c) and (d)) ST_1, and ((e) and (f)) ST_2.

Table 1
Energy-dispersive X-ray spectroscopy (EDS) analyses of ST_1 and ST_2.

Elements	ST_1 (Atomic %)	ST_2 (Atomic %)
O	74.50	63.47
Ti	13.90	14.63
Si	5.23	6.29
Na	3.24	8.99
Al	0.89	2.03
Ca	0.84	0.79
Fe	1.00	0.75
Mg	0.40	0.24
Zr	–	0.56
Cl	–	1.93
S	–	0.2
K	–	0.11

various surface morphologies. The SEM images of ST_1 found the TiO_2 sheets were converted into a TiO_2 rod shape that was evenly dispersed on the surface of the sludge. In contrast, the SEM images of ST_2 showed that TiO_2 rods with pores accumulated as layers on the surface of samples. The formation of the porous structure of the catalyst may have resulted from the presence of organic matter in SS, which was volatilized into a gas at a high temperature in the muffle furnace. Previous research has reported that thermal-alkaline pretreatment can improve the adsorption properties of sludge-based biochar [27]. The greater degree of the porous structure of the catalyst indicates high adsorption ability and degradation efficiency in the aqueous wastewater treatment. Compared with the results of previous studies, our research found that these catalytic materials had different surface morphologies, which could have resulted from different preparation methods and different properties of SS.

Table 1 shows the elemental analysis results of the sludge-TiO_2 photocatalyst samples (ST_1 and ST_2) by means of EDS analysis. The main elements of O, Ti, Si, Al, Fe, and Ca were detected with an atomic ratio of 74.50%: 13.90%: 5.23%: 0.89%: 1.00%: 0.84% in ST_1, and with an atomic ratio of 63.47%: 14.63%: 6.29%: 2.03%: 0.75%: 0.79% in ST_2. Moreover, more non-metal elements were found in the ST_2. These results indicate that the inorganic materials and transition metals existed in both catalytic materials, which might improve their photocatalytic abilities. Composites of the inorganic material and transition metals with TiO_2 have previously revealed an improvement over TiO_2 in their optical absorption over TiO_2, in addition to degradation of organic compounds, and the hydrophilicity of the material surface [28–30]. In addition, the difference in the atomic ratio between ST_1 and ST_2 could be the reason for their contrasting chemical compositions and crystalline phases. Compared with the element analyses of other particles, the differences in sludge properties between ST_1 and ST_2 were significant, which might lead to different catalytic properties.

3.2. Crystal structure of sludge-derived TiO_2 photocatalysts

Fig. 2 illustrates the XRD patterns of TiO_2, ST_0, ST_1, and ST_2 samples. According to TiO_2, peaks at 2θ value at 27.4°, 54.3° and 69.8° were indexed to (1 1 0), (2 1 1), and (1 1 2) crystal plane of rutile TiO_2 (JCPDS Card No. 72-1148), respectively, whereas peaks at 2θ value at 25.3° and others were assigned to anatase TiO_2 (JCPDS Card No. 04-0447).

After the thermal-alkaline pretreatment, Hydrogen Titanium Oxide Hydrate $H_2Ti_5O_{11}{\cdot}H_2O$ (JCPDS Card No. 44-0131), Carbon C60 and organic matters $C_{15}H_{10}O_2$ ((JCPDS Card No. 49-2059) was detected in ST_2. With thermal-alkaline and high-pressure pretreatment, TiO_2 can be transformed to $H_2Ti_5O_{11}{\cdot}H_2O$ [25], and sludge-based activated carbon is obtained during this process [27]. Heating treatment at 600 °C for 0.5 h under air and nitrogen gas protection resulted in several broad diffraction peaks of sodium- magnesium titanium oxide ($Na_{0.7}Mg_{0.35}Ti_{1.7555}O_4$, JCPDS Card No. 37-0545) and rutile TiO_2 in

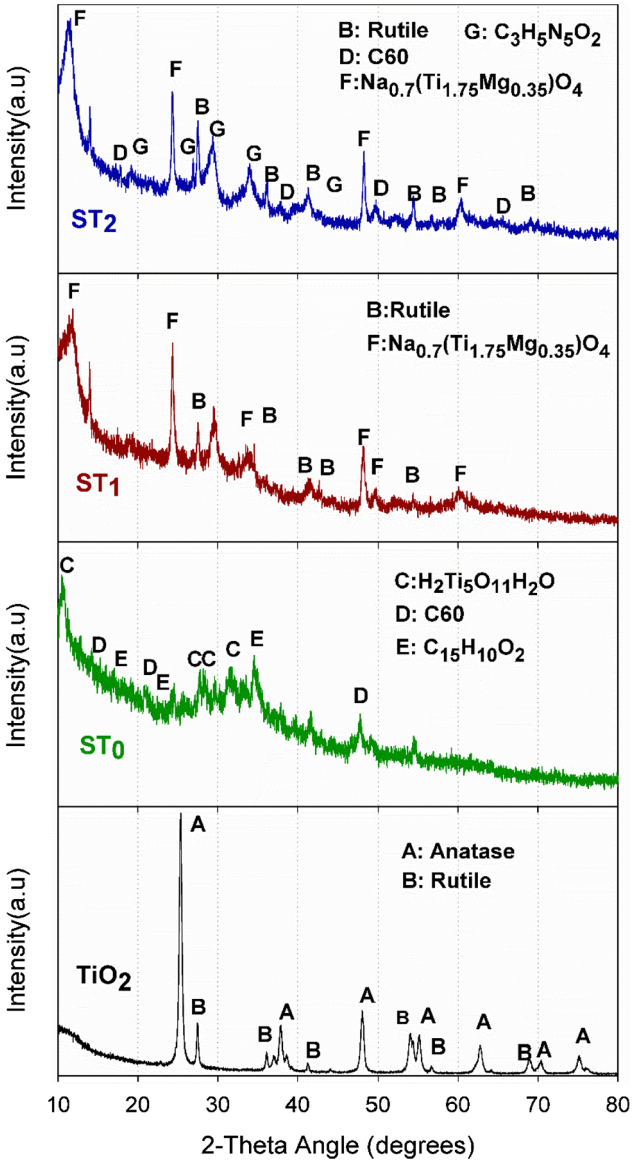

Fig. 2. X-ray diffraction (XRD) patterns of TiO_2, ST_1, and ST_2 samples.

both ST_1 and ST_2. This indicated the transition metals doped on the TiO_2 lattice in ST_1 and ST_2. The diffraction peaks were at 27.470°, 36.019°, 41.197°, 54.315°, 56.701°, and 69.033° which were assigned to the (1 1 0), (1 0 1), (1 1 1), (2 1 1), (2 2 0), and (3 0 1) planes of TiO_2 (JCPDS Card No. 05-0628), respectively. Temperatures above 400 °C result in the anatase TiO_2 crystalline structure to will change slowly to rutile until all the anatase has completely disappeared [2]. In addition, the diffraction peaks of carbon (JCPDS Card No. 46-0943) appeared at 45.545°, 48.375°, and 75.232° in ST_2. These peaks might be due to the decomposition of the carbonaceous materials at 600 °C in the N_2 atmosphere, thus generating the carbon nano [31]. Carbonaceous material can be oxidized at ambient air in and calcined at 600 °C to produce and release carbon dioxide or carbon monoxide. In comparison with ST_2, ST_1 displayed a greater number of impure peaks due to the presence of oxygen, which was confirmed by the elemental analyses in Table 1. The presence of porous carbon peaks can facilitate the improvement of adsorption within the treatment of polluting substances in the aqueous solution and further facilitate the removal of contaminants in the following catalyst experiments [32]. The SEM and EDS analyses supported the presence of pores (Fig. 1 and Table 1).

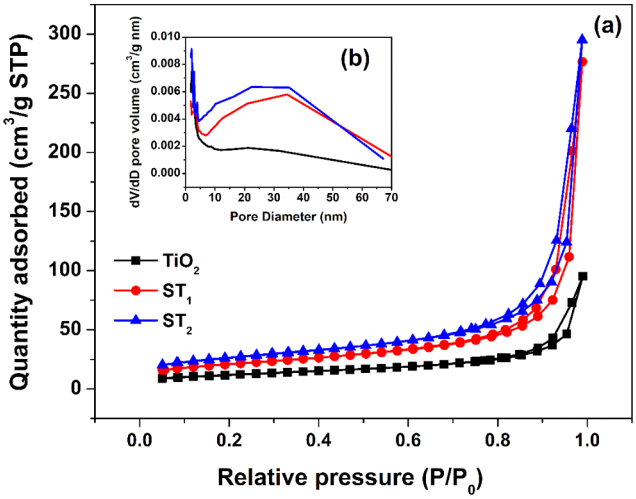

Fig. 3. (a) N_2 adsorption-desorption isotherms and (b) Pore size distributions of the samples.

3.3. Adsorption–desorption kinetics of sludge-derived TiO_2 photocatalysts

Fig. 3a shows the N_2 adsorption–desorption isotherms of the samples and Fig. 3b shows the corresponding pore size distribution curves. According to the International Union of Pure and Applied Chemistry (IUPAC) classification, the isotherm patterns of TiO_2, ST_1, and ST_2 can be classified as type-IV with an H3 hysteresis loop which indicates a mesoporous structure [33]. The mesopores of TiO_2 mainly originated from the interspaces of the aggregated nanoparticles or slit-like pores formed by the aggregates of irregular particles [34]. The pore size distributions of the samples (Fig. 3b) confirmed the predominance of the mesoporous form. The BET surface area and the pore volume of ST_2 was 92.97 $m^2\ g^{-1}$ and 0.46 cm^3/g (n = 2), which were larger than the corresponding values for ST_1 (73.78 $m^2\ g^{-1}$ and 0.46 cm^3/g, n = 2) and TiO_2 (42.45 $m^2\ g^{-1}$ and 0.15 cm^3/g, n = 2). These characteristics for ST_2 resulted from the increased number and volume of pores, which was is supported by the SEM analysis. Meanwhile, the pore size of TiO_2, ST_1 and ST_2 was 10.89 nm, 23.31 nm and 20.02 nm (n = 2), respectively, implying all the photocatalysts have mesopore structure. According to a previous study [11], the BET surface area of the sludge-TiO_2 catalytic material was 140 $m^2\ g^{-1}$, which is larger than that of pure TiO_2 (130 $m^2\ g^{-1}$) and this was attributed to the increased number and volume of pores. In our study, the surface area of TiO_2 was 42.45 $m^2\ g^{-1}$ and the BET surface of our sludge-TiO_2 catalytic materials, ST_1 and ST_2, increased by approximately 73.8% and 119.0%, respectively. This proportional increase is much larger than that reported by Wang et al. [11].

3.4. UV–Vis diffuse reflectance spectra of sludge-derived TiO_2 photocatalysts

UV–Vis diffuse reflectance spectra of the samples are compared in Fig. 4a. TiO_2 from the municipal SS possessed higher light absorption intensity and a larger absorption edge compared with the primitive P25 TiO_2. There was an increase in the absorption spectra intensity of the sample ST_2 to a level even higher than that of the original TiO_2. Consequently, the product ST_2 could assimilate a greater amount of energy from visible light illumination than the original TiO_2. Fig. 4b compares shows the prepared photocatalytic material with TiO_2 particles using FT-IR, which illustrates a larger number of peaks after calcination. The absorption peaks of ST_1 and ST_2 ranged from 700 cm^{-1} to 450 cm^{-1},

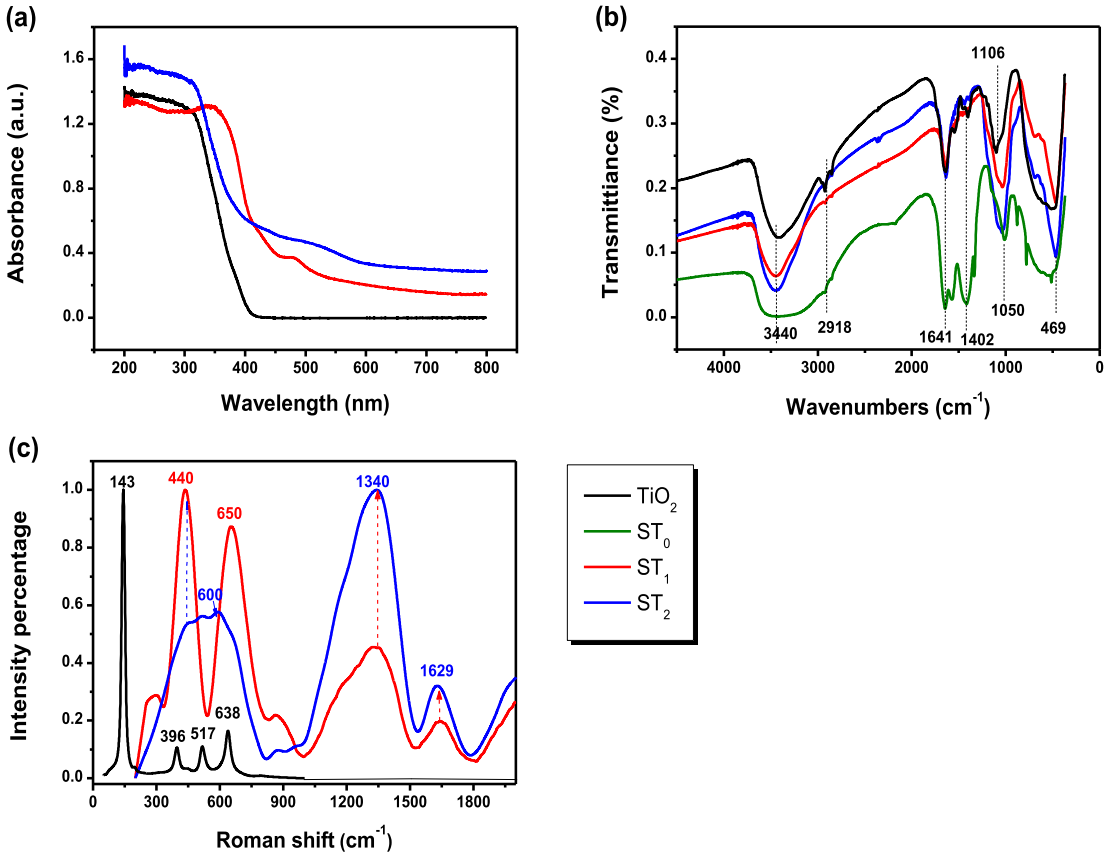

Fig. 4. (a) Ultraviolet–visible (UV–Vis) diffuse reflectance spectra of the three materials, (b) Fourier transform infrared (FT-IR) spectra of the samples TiO_2, ST_1, and ST_2, (c) Raman spectroscopy of the samples TiO_2, ST_1, and ST_2.

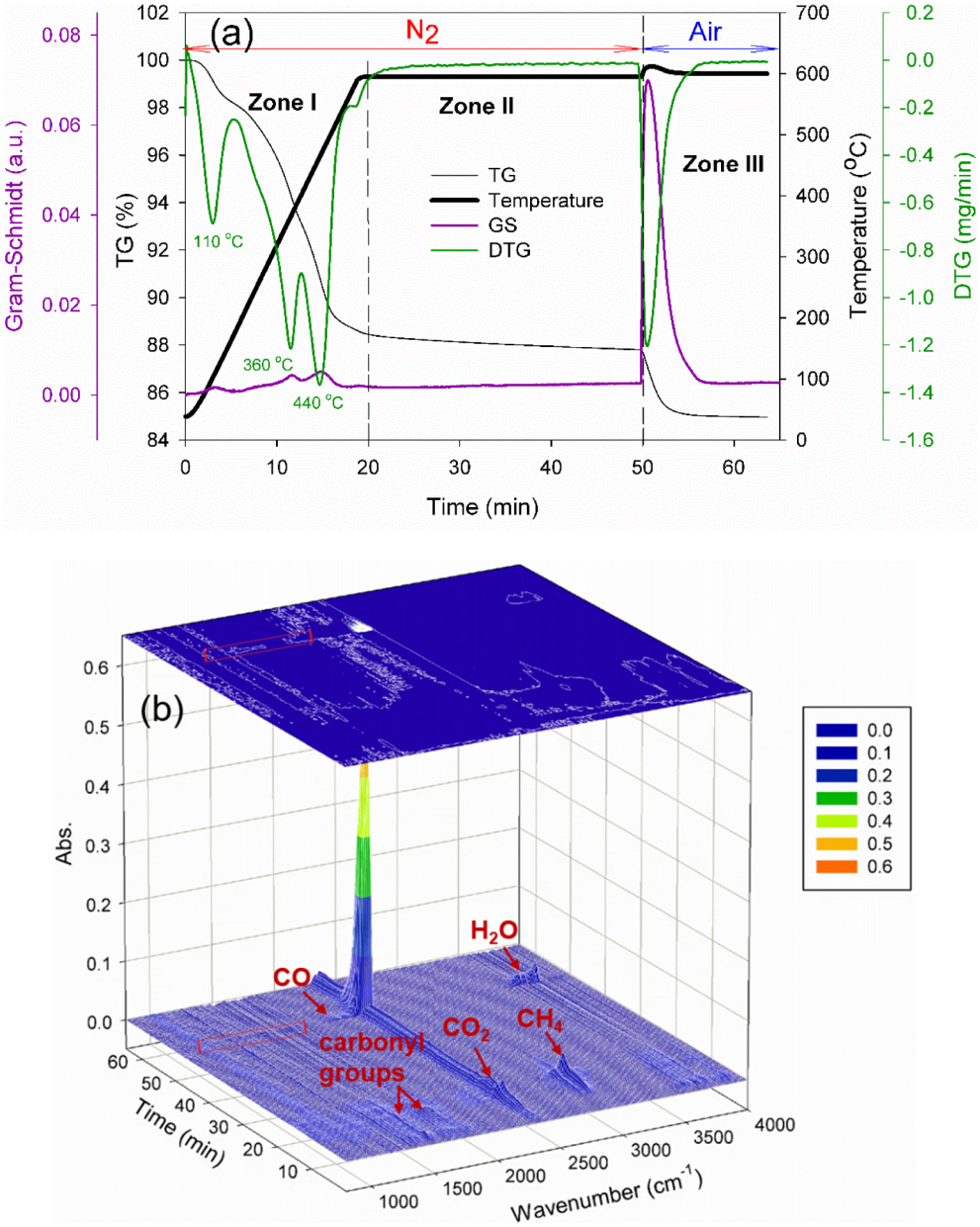

Fig. 5. (a) TG, temperature profile, DTG, and Gram-Schmidt signal curves, and (b) three-dimensional FT-IR spectra of evolved gases of the mixture of sludge-TiO_2 during the heating with N_2 and air atmosphere.

which represent the absorption and vibration of Ti-O-Ti bonds, and the characteristic peak of TiO_2 was sharper than that found by [35,36]. The broad bands centred at approximately 3400 cm^{-1} and 1630 cm^{-1} can be attributed to the stretching vibration of hydrogen-bonded hydroxyl groups of water –OH stretching [37]. The sludge-TiO_2 photocatalysts presented two well-defined bands at 2920 cm^{-1} and 2850 cm^{-1} assigned to the asymmetric and symmetric stretching vibrations of $–CH_2–$ and $CH_3–$ in alkyl chains, as well as bands in the range of 1 00–1500 cm^{-1} which is attributed to CH_2 bending vibrations [36]. In addition, the band at 1030 cm^{-1} refers to the stretching vibration of C–O–C and vibrations of silica (Si–O–Si), which indicates the presence of oxygen functional groups on the surface and SiO_2 in ST_1 and ST_2 [38,39], whereas the 1140 cm^{-1} band in the TiO_2 can be related to the vibration of –COOTi [36]. Carbon doping in TiO_2 lattice could lower the TiO_2 band gap of and enhance absorption in the visible region [40].

As mentioned, the sludge-TiO_2 photocatalysts contained a greater number of organic functional groups after combining with SS compared with TiO_2. The Raman spectra ofTiO_2, ST_1, and ST_2 in Fig. 4c shows an increase in the characteristic band intensity. The formation of TiO_2 and the anatase-to-rutile phase transition were further confirmed by Raman spectroscopy [41]. The presence of four Raman active modes in TiO_2 was identified at 143 cm^{-1}, 396 cm^{-1}, 517 cm^{-1}, and 638 cm^{-1} [42]. Peaks at 143 cm^{-1}, 396 and 517 cm^{-1} belong to the anatase phase, whereas those at 447 and 613 cm^{-1} correspond to rutile. After the thermal-alkaline process, the strong single peak at 144 cm^{-1} vanished in both ST_1 and ST_2. In contrast, the magnitude of the rutile peaks increased in ST_1 and ST_2. This suggests the transformation of anatase to rutile due to the high-temperature heating.

All curves exhibited two relatively broad bands at Raman shifts of 1340 cm^{-1} and 1640 cm^{-1}, which correspond to the D-band and G-band of carbons, respectively. The D-band is be labelled as the amorphous or disordered graphite, whereas the G-band indicates the presence of graphitic crystallites [43,44]. The graphitic degree of carbons was confirmed by the value of I_D/I_G [43–45]. The I_D/I_G ratios calculated by the integrated areas of the D-bands and G-bands of ST_1 and ST_2 were 7.79 and 10.82, respectively, implying a greater degree of isolation of

sp^2 carbon atoms and higher surface area of ST_2. The residual oxygen atoms in the biochar were involved in the crosslinking of the carbon microstructure, yielding a non-graphitizing hard carbon [43]. McDonald-Wharry obtained the I_D/I_G ratio by using graphites and regular fullerenes, and found that an increase in the I_D/I_G ratio (0.55–1.20) indicated a conversion of amorphous carbon to graphene-like carbon. In general, the growth and organization of aromatic clusters as well as carbon microstructure in the biochar samples becomes ordered and condensed at higher pyrolysis temperature [43]. Therefore, the highest surface area in ST_2 was mainly attributed to the carbonaceous graphene-like structure, which was generated by the residual non-metal materials in N_2 calcination. This finding was consistent with our analyses of BET, SEM, and XRD.

3.5. TG-IR analysis for different calcination atmospheres

The thermal decomposition process of the sludge-TiO_2 using thermogravimetric (TG), differential thermogravimetric (DTG), the Gram–Schmidt (GS) signal and the three-dimensional FT-IR spectra of evolved gases curves are described in this section. As shown in Fig. 5a, indicates that the thermal decomposition process can be divided into three main zones. The first zone ranged from room temperature to 600 °C under the N_2 atmosphere, with a recorded mass loss was recorded at about 11% of the initial sludge-TiO_2. Three peaks of DTG and GS most likely correspond to the evaporation of water remaining after sample drying and the degradation of organic materials in the sludge [46]. The second zone with a constant 600 °C temperature for 30 min resulted in significantly lower mass loss rates, indicating decomposition of inorganic materials, including the residual ash (e.g., calcium carbonate) and carbonaceous matter [47]. The third zone led to a mass loss of about 3%, contributed mainly by the burning of carbonaceous matters. Fig. 4b shows the evolution of the evolved gas from the thermal decomposition process of the sludge-TiO_2. The main gases identified by the characteristics wave numbers were H_2O (4000–3600 and 2100–1200 cm^{-1}), CH_4 (3100–2800 cm^{-1}), CO_2 (2400–2250 cm^{-1}), CO (2250–2000 cm^{-1}) and small molecule lipids, aldehydes and acids (1900–1200 cm^{-1}) [48–50]. Gases such as NO_x, including NO (1762 cm^{-1}), NO_2 (1520 cm^{-1}) and SO_2 (1342 cm^{-1}) were also detected, although the intensity of these gases was relatively lower. According to SEM analysis, H_2O was generated during zones I and III due to the evaporation of water and burning of the hydrocarbon, while the emission of carbonyl groups, CO_2 and CH_4 can be attributed to the decomposition of organic matters in the sludge. Moreover, the burning of the calcination residues of sludge-TiO_2 resulted in the emission of CO_2, CO, and a small amount of NO, NO_2 and SO_2, indicating that the N_2 calcination atmosphere could reserve some organic matter containing C, N, and S elements. As mentioned above, the sludge-TiO_2 calcination in the air can release a large amount of CO_2, CO, NO_x and SO_2, which can cause air pollution. However, the sludge-TiO_2 calcination in the N_2 atmosphere could produce energy carrier materials like gases and bio-oil for energy recovery from dried sewage sludge with volatile content (85.5%).

3.6. Photo-catalytic ability under visible light irradiation

To investigate the photocatalytic activities of TiO_2, ST_1, and ST_2, the decomposition of tetracycline with the aqueous solution was conducted under visible light ($\lambda \geq 400$ nm). The illumination was provided by an 800 W Xe lamp and the results are shown in Fig. 6a. After irradiation of 120 min, the removal rate of ST_2 reached 76.3%, which was higher than those of ST_1 (56.8%) and P25 TiO_2 (36.1%). The photocatalytic experiments were repeated for two times with the same catalyst. After each experiment, the catalyst was centrifuged, washed, and dried under 150 °C for about 3 h. No obvious decrease of photocatalytic activity is found in this experiment. This result was nearly twice as large as that of the original TiO_2 and can be associated with different textural properties of the materials. Compared with initial TiO_2 and ST_1 (Fig. 6a), ST_2 presented better photocatalytic activity under invisible light for antibiotic wastewater treatment as well as more efficient transport pathways for molecular trafficking. On the basis of Fig. 6, it is inferred that the reduction of tetracycline by using sludge-TiO_2 is feasible. Thorough analysis of the presence and evolution of intermediates and the economic feasibility of photocatalysts due to the photocatalytic treatment of tetracycline requires further investigation, preferably on a continuous and larger-scale experiment.

The photocatalytic abilities of ST_1 and ST_2 were estimated on the basis of the kinetic data for the degradation of tetracycline under visible light irradiation. The curve was fitted according to the first kinetic and the second kinetic orders to investigate the kinetic behaviour of photodegradation tetracycline over ST_1 and ST_2. The outside lines are the first kinetic curves, and the inset in Fig. 6 is the second kinetic curve [51]. The first kinetic equation is as follows:

$$\ln(C/C_0) = kt, \quad (1)$$

where C is the concentration of tetracycline (mg L^{-1}) at time t (min), C_0 is the concentration of tetracycline (mg L^{-1}) at t = 0 (min), and k is the reaction rate constant (min^{-1}). The constant rate k can be determined from the slope of the linear plot. The second kinetic equation is as follows [51]:

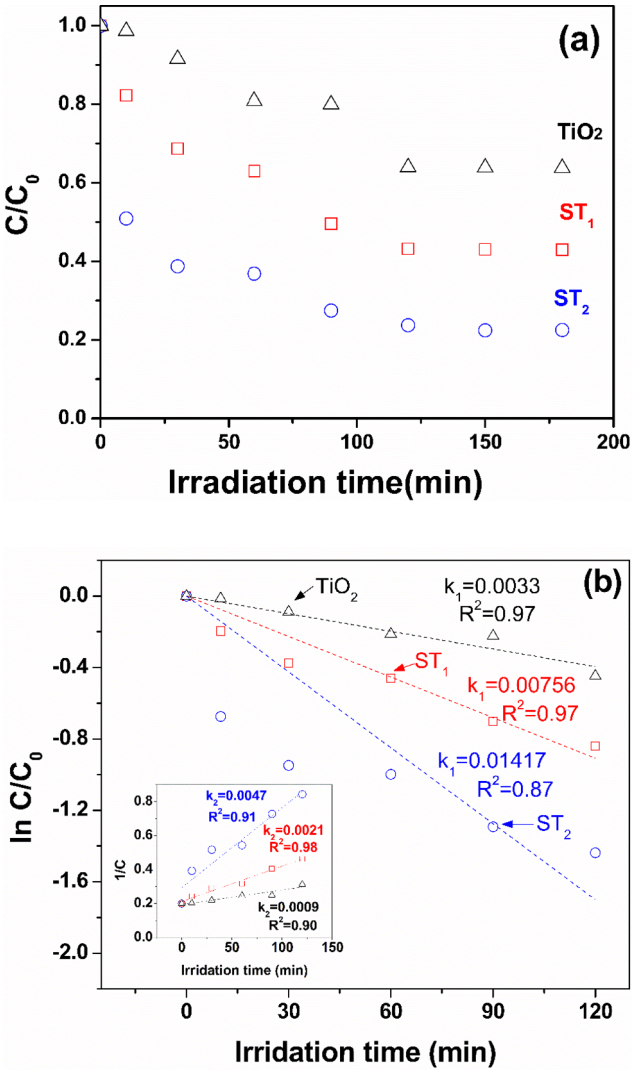

Fig. 6. (a) C/C_0 conversion plots of tetracycline over the samples under visible light irradiation, (b) degradation kinetics of tetracycline under visible light irradiation.

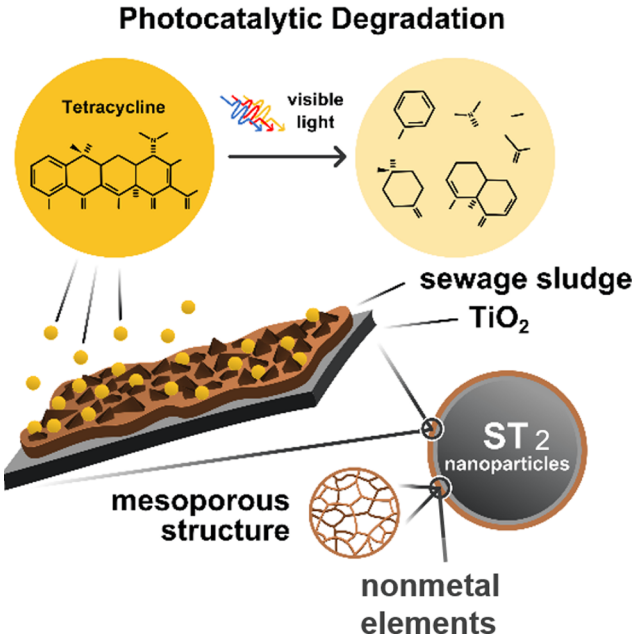

Fig. 7. A conceptual explanation for the higher photo-activity of ST_2 compared with ST_1 and TiO_2.

$$1/c = kt + b \quad (2)$$

The results in Fig. 6 show that the constant rate k values of ST_2 composites were higher than those of ST_1 and TiO_2 in the first and the second kinetic equations, and this indicates that the photocatalytic activity of ST_2 was superior to that of ST_1. The values of the second kinetic linear regression coefficients (R^2) of ST_2 and ST_1 were higher than the first kinetic linear regression coefficients, indicating that the second kinetic equation better represented the process of degradation.

A conceptual explanation for the higher photo-activity of ST_2 compared with ST_1 and TiO_2 for the TC degradation is illustrated in Fig. 7. Initially, TiO_2 supported the municipal SS in ST_2 and led to a large organic surface structure. Initially, TiO_2 supported the municipal SS in ST_2 and led to a large organic surface structure. The heterogeneous functional group and microstructure on the surface increased the adsorption opportunity for TC compound in the solution. Then, the transition metals and carbon dopants could be present in ST_2, will facilitate the generation of the electron-hole pairs and fasten the electron transfer from e_{cb-} to h_{vb+} by the visible light irradiation of ST_2. This step will lead to the degradation of the recalcitrant compounds (aromatics) and convert them to more simple intermediate compounds (benzene derivates, phenolic compounds, tributyl phosphate and heptadecane, etc.) [52]. Then, the photo-generated electrons and electron acceptors such as O_2 and H_2O ($\cdot O^{2-}$ and $\cdot OH$) can synergistically degrade the aromatics and intermediate compounds to carbon dioxide and water in the end.

4. Conclusions

Novel sludge-derived TiO_2 photocatalysts were synthesized through a thermal-alkaline process in the air (ST_1) and N_2 (ST_2). ST_2 exhibited higher surface area and crystallinity than ST_1 and TiO_2 due to the residual non-metal material of the calcination in N_2. Meanwhile, ST_2 showed higher photocatalytic activity than other materials, which was contributed to better pollutants and visible light absorption and faster electron–hole pair separation efficiency. Photocatalytic degradation of tetracycline by ST_2 followed the second kinetic equation, with the highest removal rate reaching 80% after 2 h (5 mg L^{-1} of TC, 10 mg L^{-1} of ST_2). This research has shown the feasibility to synthesize excellent sludge-derived TiO_2 photocatalysts, providing a promising and eco-friendly method to resource reutilization of waste sludge and degradation of antibiotics.

Acknowledgements

This work was sponsored by the National Natural Science Foundation of China (No. 21507079, 51808226), the State Key Laboratory of Pollution Control and Resource Reuse Foundation (No. PCRRF14007), the Science & Technology Innovation Action Plan of Shanghai under the Belt and Road Initiative (No. 17230741100), the Distinguished Professor in Universities of Shanghai (Oriental Scholar, No. TP2017041), the Shanghai Pujiang Program (No. 17PJ1402100), the Fundamental Research Funds for the Central Universities (No. 40500-20101-222001, 40500-20101-222078, 13903-120215-10435), and Shanghai Institute of Pollution Control and Ecological Security.

Appendix A. Supplementary data

Supplementary data to this article can be found online at https://doi.org/10.1016/j.fuel.2019.04.093.

References

[1] Hadi P, Xu M, Ning C, Lin CSK, McKay G. A critical review on preparation, characterization and utilization of sludge-derived activated carbons for wastewater treatment. Chem Eng J 2015;260:895–906.
[2] Zhou ZY, Zhang YX, Wang HT, Chen T, Lu WJ. Enhanced photodegradation of pentachlorophenol in a soil washing system under solar irradiation with TiO2 nanorods combined with municipal sewage sludge. Micropor Mesopor Mater 2015;201:99–104.
[3] Chung WJ, Nguyen DD, Bui XT, An SW, Banu JR, Lee SM, et al. A magnetically separable and recyclable Ag-supported magnetic TiO2 composite catalyst: fabrication, characterization, and photocatalytic activity. J Environ Manage 2018;213:541–8.
[4] Zielinska A, Oleszczuk P, Charmas B, Skubiszewska-Zieba J, Pasieczna-Patkowska S. Effect of sewage sludge properties on the biochar characteristic. J Anal Appl Pyrol 2015;112:201–13.
[5] Koncewicz-Baran M, Orlowska K, Gondek K. Characteristics of selected fractions of heavy metals in biologically and thermally transformed sewage sludge. Desalin Water Treat 2014;52(19–21):3783–9.
[6] Tu YC, Lim H, Chang CY, Shyue JJ, Su WF. Enhancing performance of P3HT:TiO2 solar cells using doped and surface modified TiO2 nanorods. J Colloid Interface Sci 2015;448:315–9.
[7] Sun B, Zhou GW, Zhang Y, Liu RR, Li TD. Photocatalytic properties of exposed crystal surface-controlled rutile TiO2 nanorod assembled microspheres. Chem Eng J 2015;264:125–33.
[8] Huang ZW, Cui F, Kang HX, Chen J, Xia CG. Characterization and catalytic properties of the CuO/SiO2 catalysts prepared by precipitation-gel method in the hydrogenolysis of glycerol to 1,2-propanediol: effect of residual sodium. Appl Catal A-Gen 2009;366(2):288–98.
[9] Bartkowska I. Influence of the sewage sludge stabilization process on the value of its oxidation-reduction potential. Environ Technol 2014;35(17):2160–6.
[10] Periyat P, Saeed PA, Ullattil SG. Anatase titania nanorods by pseudo-inorganic templating. Mater Sci Semicond Process 2015;31:658–65.
[11] Wang XP, Huang SQ, Zhu NW, Lou ZY, Yuan HP. Facile synthesis of porous TiO2 photocatalysts using waste sludge as the template. Appl Surf Sci 2015;359:917–22.
[12] Fuerte A, Hernandez-Alonso MD, Maira AJ, Martinez-Arias A, Fernandez-Garcia M, Conesa JC, et al. Visible light-activated nanosized doped-TiO2 photocatalysts. Chem Commun 2001;24:2718–9.
[13] Tsui LK, Nguyen NT, Wang L, Kirchgeorg R, Zangari G, Schmuki P. Hierarchical decoration of anodic TiO2 nanorods for enhanced photocatalytic degradation properties. Electrochim Acta 2015;155:244–50.
[14] Gao Q, Wu XM, Fan YM, Zhou XY. Fabrication of hierarchically structured rutile TiO2 nanorods on mica particles and their superhydrophilic coating without UV irridiation. Appl Surf Sci 2014;289:281–8.
[15] Xie Z, Liu XX, Wang WP, Wang XJ, Liu C, Xie Q, et al. Enhanced photoelectrochemical and photocatalytic performance of TiO2 nanorod arrays/CdS quantum dots by coating TiO2 through atomic layer deposition. Nano Energy 2015;11:400–8.
[16] Zhu XD, Wang YJ, Sun RJ, Zhou DM. Photocatalytic degradation of tetracycline in aqueous solution by nanosized TiO2. Chemosphere 2013;92(8):925–32.
[17] Lin Y, Ma X, Peng X, Yu Z, Fang S, Lin Y, et al. Combustion, pyrolysis and char CO2-gasification characteristics of hydrothermal carbonization solid fuel from municipal solid wastes. Fuel 2016;181:905–15.
[18] Ben W, Qiang Z, Pan X, Chen M. Removal of veterinary antibiotics from sequencing batch reactor (SBR) pretreated swine wastewater by Fenton's reagent. Water Res 2009;43(17):4392–402.
[19] Yao LL, Wang YX, Tong L, Li YG, Deng YM, Guo W, et al. Seasonal variation of antibiotics concentration in the aquatic environment: a case study at Jianghan Plain, central China. Sci Total Environ 2015;527:56–64.

[20] Cheng DL, Ngo HH, Guo WS, Chang SW, Nguyen DD, Kumar SM, et al. Problematic effects of antibiotics on anaerobic treatment of swine wastewater. Bioresour Technol 2018;263:642–53.
[21] Homem V, Santos L. Degradation and removal methods of antibiotics from aqueous matrices – a review. J Environ Manage 2011;92(10):2304–47.
[22] Cheng DL, Ngo HH, Guo WS, Liu YW, Zhou JL, Chang SW, et al. Bioprocessing for elimination antibiotics and hormones from swine wastewater. Sci Total Environ 2018;621:1664–82.
[23] Nepa C. Water and Wastewater Monitoring Methods. third ed. Beijing, China: Chinese Environmental Science Publishing House; 1997.
[24] Zhang D. Enhanced photocatalytic activity for titanium dioxide by co-modification with copper and iron. Transition Met Chem 2010;35(8):933–8.
[25] Yang HG, Zeng HC. Synthetic architectures of TiO2/H2Ti5O11·H2O, ZnO/H2Ti5O11·H2O, ZnO/TiO2/H2Ti5O11·H2O, and ZnO/TiO2 nanocomposites. J Am Chem Soc 2005;127(1):270–8.
[26] Zhou J, Xue X, Li Y, Zhang J, Chen F, Wu L, et al. Multiresidue determination of tetracycline antibiotics in propolis by using HPLC-UV detection with ultrasonic-assisted extraction and two-step solid phase extraction. Food Chem 2009;115(3):1074–80.
[27] Xiao B, Dai Q, Yu X, Yu P, Zhai S, Liu R, et al. Effects of sludge thermal-alkaline pretreatment on cationic red X-GRL adsorption onto pyrolysis biochar of sewage sludge. J Hazard Mater 2018;343:347–55.
[28] Asahi R, Morikawa T, Ohwaki T, Aoki K, Taga Y. Visible-light photocatalysis in nitrogen-doped titanium oxides. Science 2001;293(5528):269–71.
[29] Rahimpour A, Madaeni SS, Taheri AH, Mansourpanah Y. Coupling TiO2 nanoparticles with UV irradiation for modification of polyethersulfone ultrafiltration membranes. J Membr Sci 2008;313(1–2):158–69.
[30] Wu JCS, Chen C-H. A visible-light response vanadium-doped titania nanocatalyst by sol–gel method. J Photochem Photobiol, A 2004;163(3):509–15.
[31] Yu LL, Zhong Q. Preparation of adsorbents made from sewage sludges for adsorption of organic materials from wastewater. J Hazard Mater 2006;137(1):359–66.
[32] Hale SE, Lehmann J, Rutherford D, Zimmerman AR, Bachmann RT, Shitumbanuma V, et al. Quantifying the total and bioavailable polycyclic aromatic hydrocarbons and dioxins in biochars. Environ Sci Technol 2012;46(5):2830–8.
[33] Yang HQ, Han XJ, Li G, Wang YW. N-Heterocyclic carbene palladium complex supported on ionic liquid-modified SBA-16: an efficient and highly recyclable catalyst for the Suzuki and Heck reactions. Green Chem 2009;11(8):1184–93.
[34] Yu JG, Yu JC, Leung MKP, Ho WK, Cheng B, Zhao XJ, et al. Effects of acidic and basic hydrolysis catalysts on the photocatalytic activity and microstructures of bimodal mesoporous titania. J Catal 2003;217(1):69–78.
[35] Lopez T, Sanchez E, Bosch P, Meas Y, Gomez R. FTIR and UV-Vis (diffuse reflectance) spectroscopic characterization of TiO2 sol-gel. Mater Chem Phys 1992;32(2):141–52.
[36] Wang JQ, Wang JF, Sun QL, Wang W, Yan ZY, Gong WJ, et al. UV and solar light degradation of dyes over mesoporous crystalline titanium dioxides prepared by using commercial synthetic dyes as templates. J Mater Chem 2009;19(36):6597–604.
[37] Qiu YP, Ling F. Role of surface functionality in the adsorption of anionic dyes on modified polymeric sorbents. Chemosphere 2006;64(6):963–71.
[38] Smidt E, Parravicini V. Effect of sewage sludge treatment and additional aerobic post-stabilization revealed by infrared spectroscopy and multivariate data analysis. Bioresour Technol 2009;100(5):1775–80.
[39] Yuan JH, Xu RK, Zhang H. The forms of alkalis in the biochar produced from crop residues at different temperatures. Bioresour Technol 2011;102(3):3488–97.
[40] Dong F, Guo S, Wang H, Li X, Wu Z. Enhancement of the visible light photocatalytic activity of C-doped TiO2 nanomaterials prepared by a green synthetic approach. J Phys Chem C 2011;115(27):13285–92.
[41] Ma HL, Yang JY, Dai Y, Zhang YB, Lu B, Ma GH. Raman study of phase transformation of TiO2 rutile single crystal irradiated by infrared femtosecond laser. Appl Surf Sci 2007;253(18):7497–500.
[42] Ishioka K, Petek H. Raman generation of coherent phonons of anatase and rutile TiO2 photoexcited at fundamental absorption edges. Phys Rev B 2012;86(20):205201.
[43] Zhang JN, Lu F, Zhang H, Shao LM, Chen DZ, He PJ. Multiscale visualization of the structural and characteristic changes of sewage sludge biochar oriented towards potential agronomic and environmental implication. Sci Rep-Uk 2015:5.
[44] Rhim Y-R, Zhang D, Fairbrother DH, Wepasnick KA, Livi KJ, Bodnar RJ, et al. Changes in electrical and microstructural properties of microcrystalline cellulose as function of carbonization temperature. Carbon 2010;48(4):1012–24.
[45] Bokobza L, Bruneel J-L, Couzi M. Raman spectra of carbon-based materials (from graphite to carbon black) and of some silicone composites. C 2015;1(1):77.
[46] Kan T, Strezov V, Evans T. Effect of the heating rate on the thermochemical behavior and biofuel properties of sewage sludge pyrolysis. Energy Fuel 2016;30(3):1564–70.
[47] Scott SA, Dennis JS, Davidson JF, Hayhurst AN. Thermogravimetric measurements of the kinetics of pyrolysis of dried sewage sludge. Fuel 2006;85(9):1248–53.
[48] Gao N, Li J, Qi B, Li A, Duan Y, Wang Z. Thermal analysis and products distribution of dried sewage sludge pyrolysis. J Anal Appl Pyrol 2014;105:43–8.
[49] Zhang Q, Liu H, Liu P, Hu H, Yao H. Pyrolysis characteristics and kinetic analysis of different dewatered sludge. Bioresour Technol 2014;170:325–30.
[50] Chen J, Mu L, Jiang B, Yin H, Song X, Li A. TG/DSC-FTIR and Py-GC investigation on pyrolysis characteristics of petrochemical wastewater sludge. Bioresour Technol 2015;192:1–10.
[51] Lai C, Wang M-M, Zeng G-M, Liu Y-G, Huang D-L, Zhang C, et al. Synthesis of surface molecular imprinted TiO2/graphene photocatalyst and its highly efficient photocatalytic degradation of target pollutant under visible light irradiation. Appl Surf Sci 2016;390:368–76.
[52] Ahmadi M, Ramezani Motlagh H, Jaafarzadeh N, Mostoufi A, Saeedi R, Barzegar G, et al. Enhanced photocatalytic degradation of tetracycline and real pharmaceutical wastewater using MWCNT/TiO2 nano-composite. J Environ Manage 2017;186:55–63.